Subglacial carbonate deposits as a potential proxy for glacier's existence

Authors: Matej Lipar[1]*, Andrea Martín Pérez[2], Jure Tičar[1], Miha Pavšek[1], Matej Gabrovec[1], Mauro Hrvatin[1], Blaž Komac[1], Matija Zorn[1], Nadja Zupan Hajna[3], Jian-Xin Zhao[4], Mateja Ferk[1]

[1]Anton Melik Geographical Institute, Research Centre of the Slovenian Academy of Sciences and Arts, Ljubljana, 1000, Slovenia
[2]Ivan Rakovec Institute of Palaeontology, Research Centre of the Slovenian Academy of Sciences and Arts, Ljubljana, 1000, Slovenia
[3]Karst Research Institute, Research Centre of the Slovenian Academy of Sciences and Arts, Postojna, 6230, Slovenia
[4]School of Earth and Environmental Sciences, The University of Queensland, Brisbane, QLD 4072, Australia

Correspondence to: Matej Lipar (matej.lipar@zrc-sazu.si)

Supplementary Information

Supplementary Figure S1: Photographic material of the retreating Triglav Glacier (© ZRC SAZU Anton Melik Geographical Institute archive).

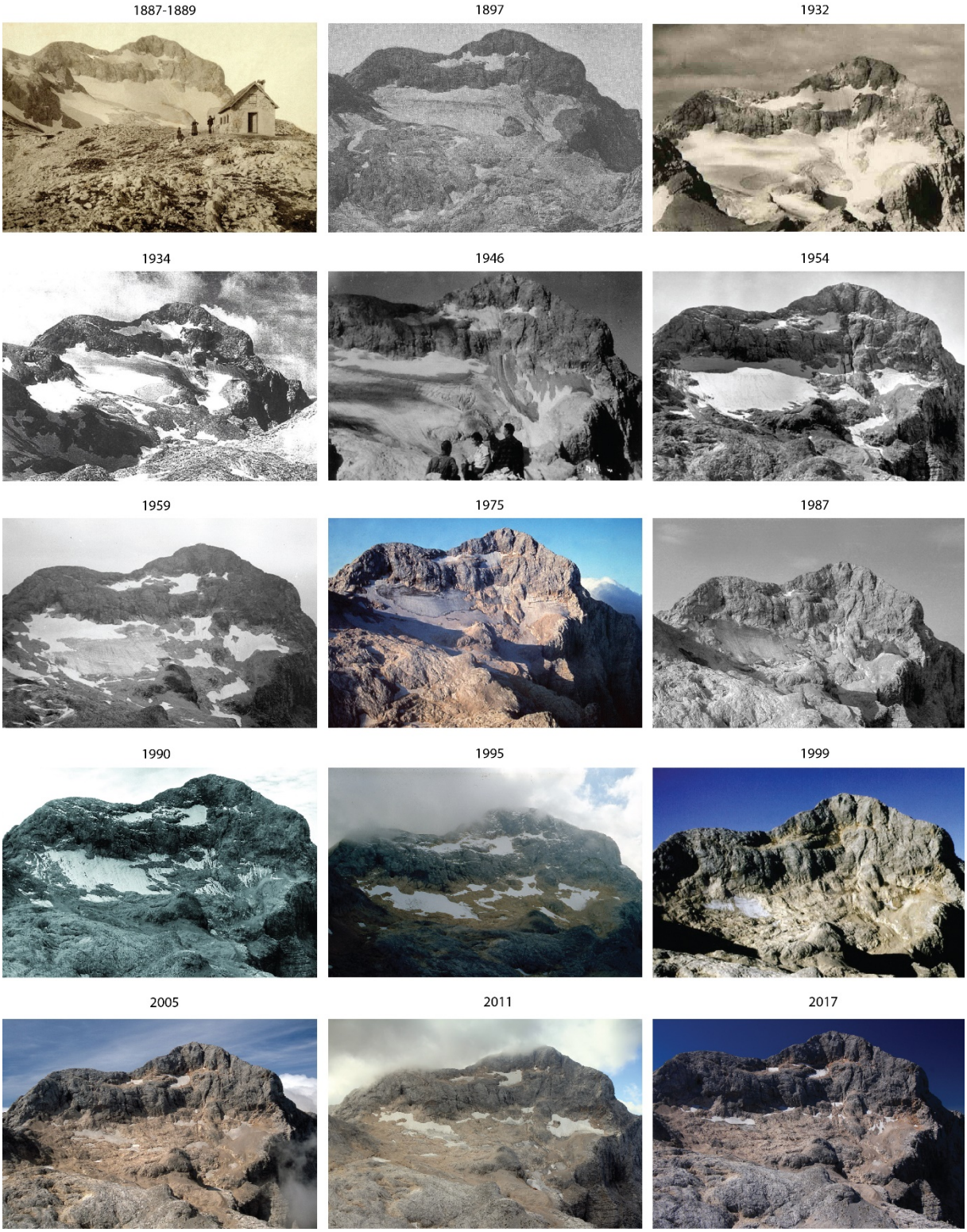

Supplementary Figure S2: The recently exposed surface with shafts and subglacial carbonate deposits (© ZRC SAZU Anton Melik Geographical Institute archive).

Supplementary Figure S3: General view of the subglacial carbonate location (© ZRC SAZU Anton Melik Geographical Institute archive).

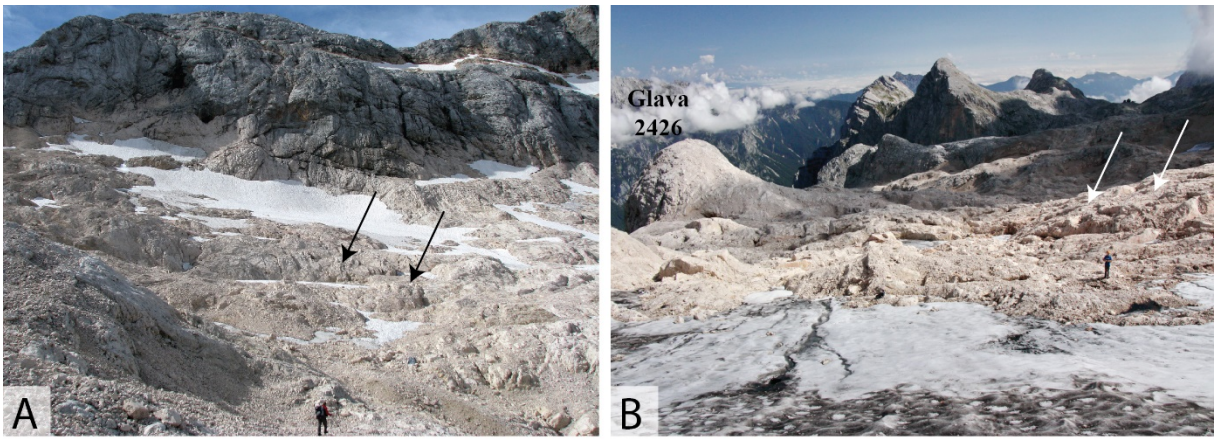

Supplementary Figure S4: Locality LiDAR DTM map of the Triglav Glacier extent and the sampling sites discussed in the text.

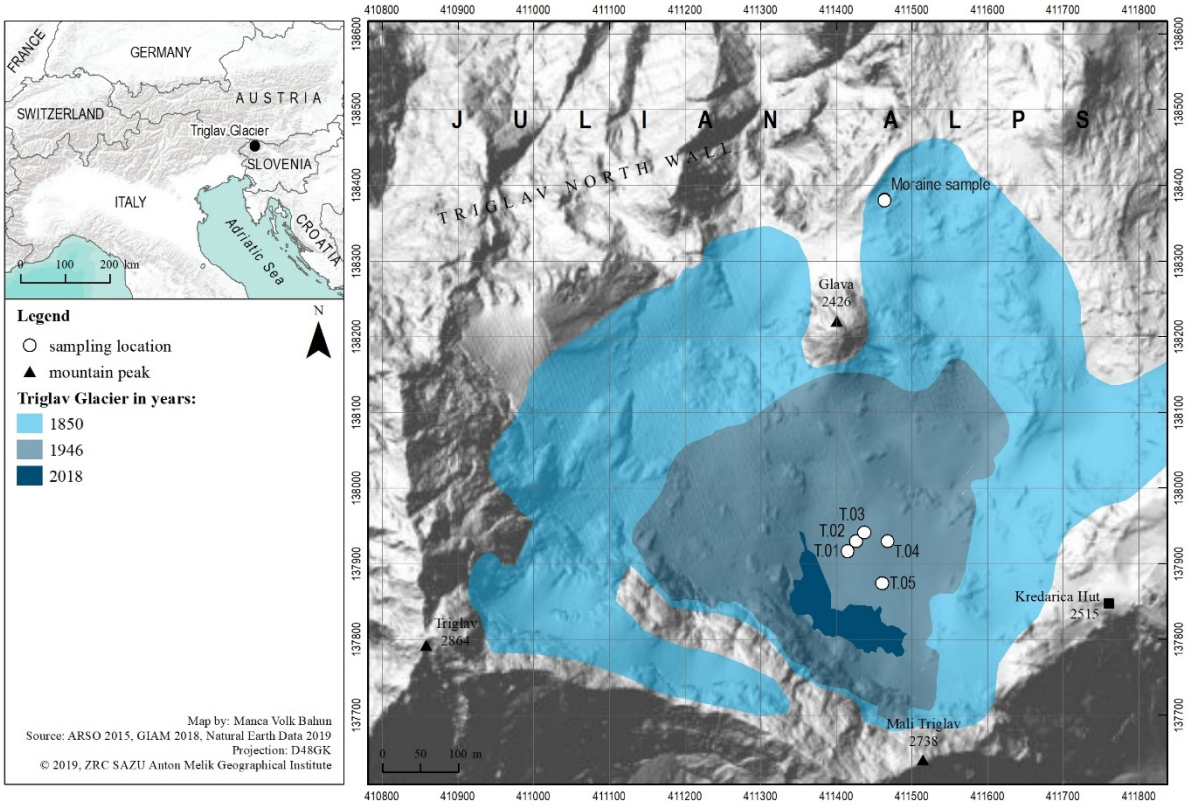

Supplementary Figure S5: Locality aerial map of the Triglav Glacier, the sampling sites discussed in the text, and general geomorphology.

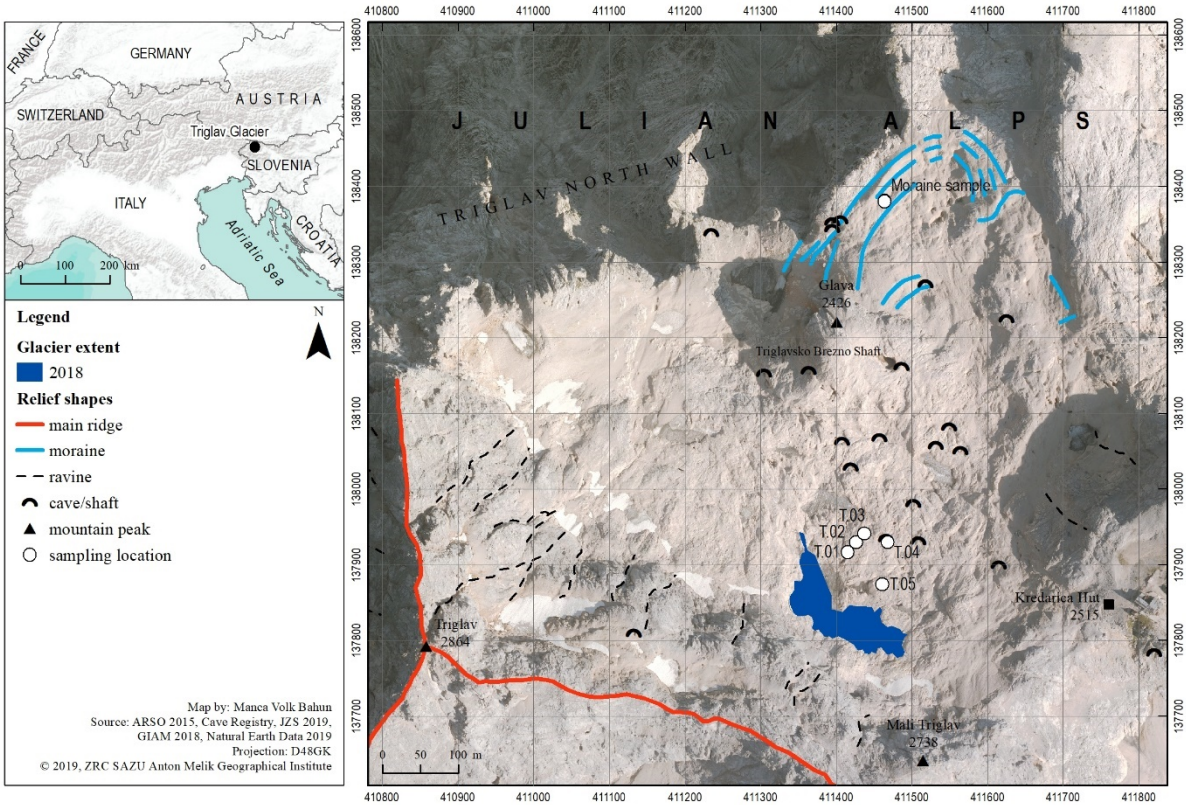

Supplementary Figure S6: Average melting season temperature (May – October) on meteorological station Kredarica (Fig. 1) between 1955 and 2018. Source: Slovenian Environment Agency.

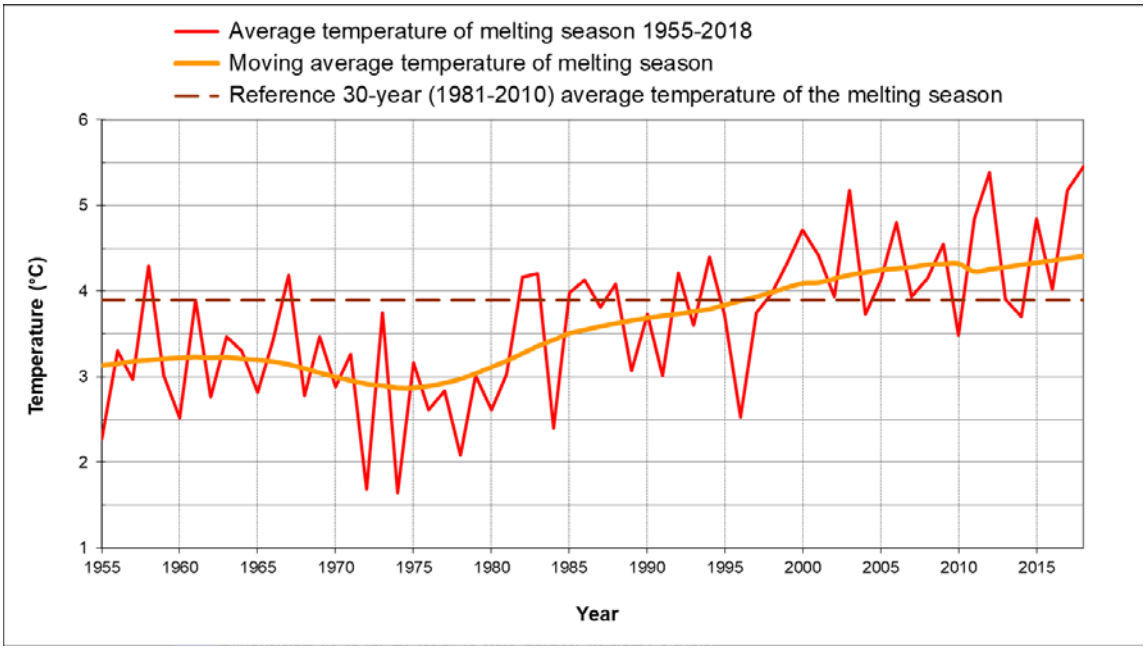

Supplementary Figure S7: Reconstruction of the highest seasonal snow height on the edge of the Triglav Glacier between 1852 and 2018. Updated from Gabrovec et al. 2014(Gabrovec et al., 2014). Source: Slovenian Environment Agency (from 1955 on), reconstruction/reanalysis before 1955 done by Jaka Ortar.

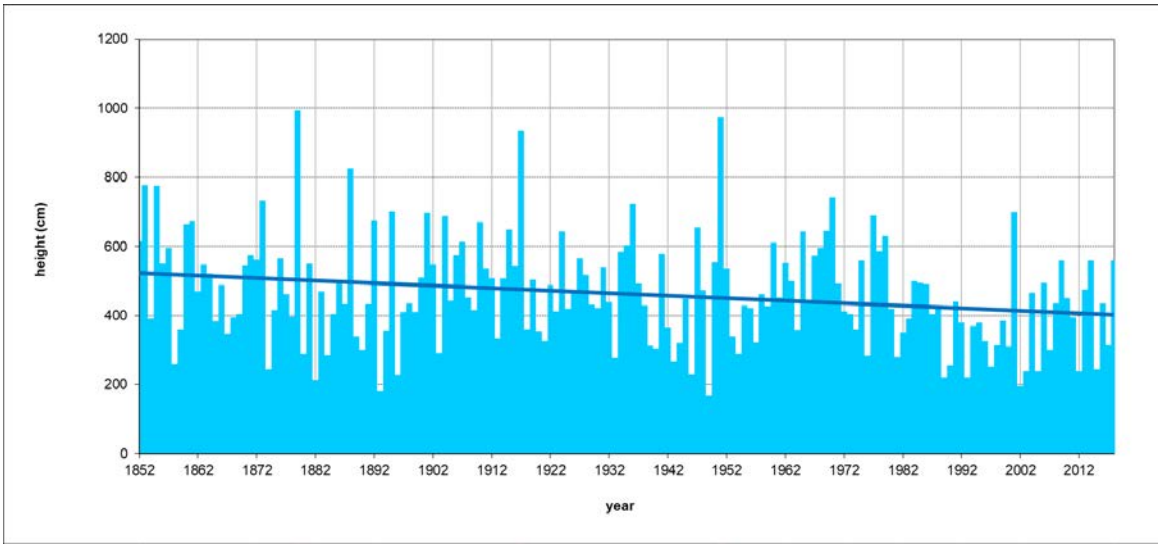

Supplementary Figure S8: XRD graphs

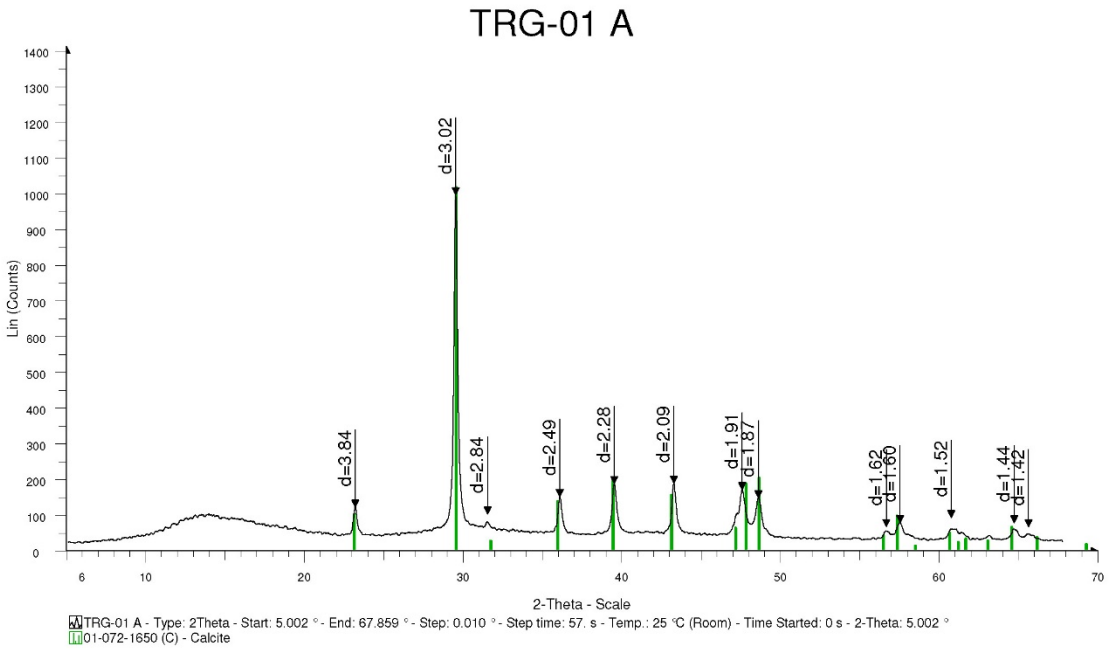

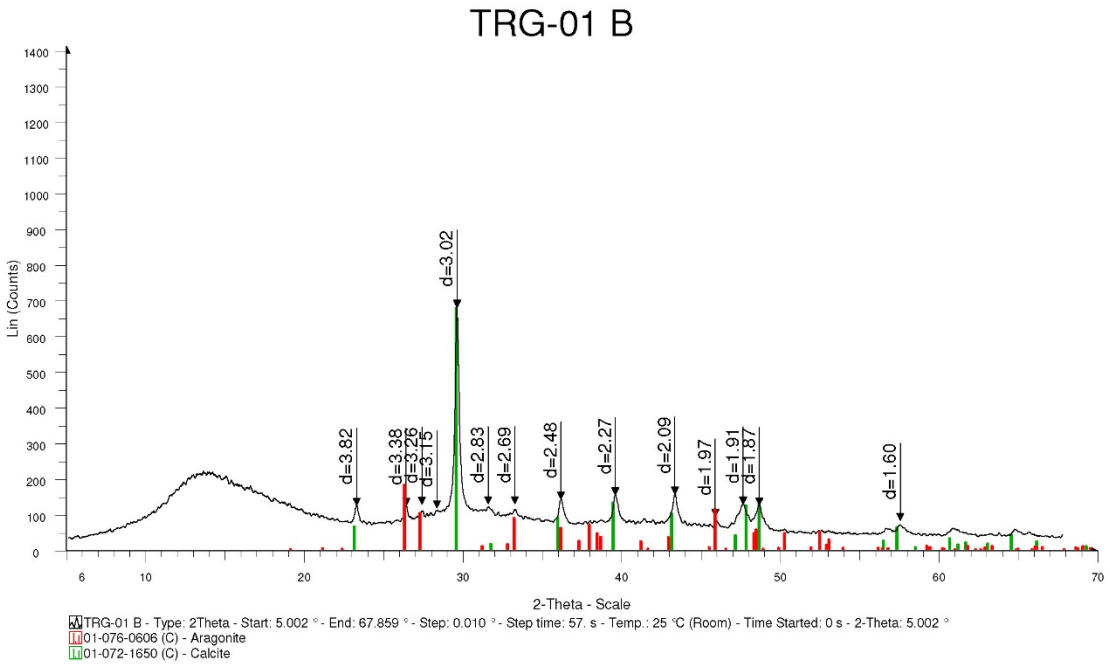

TRG-01 C

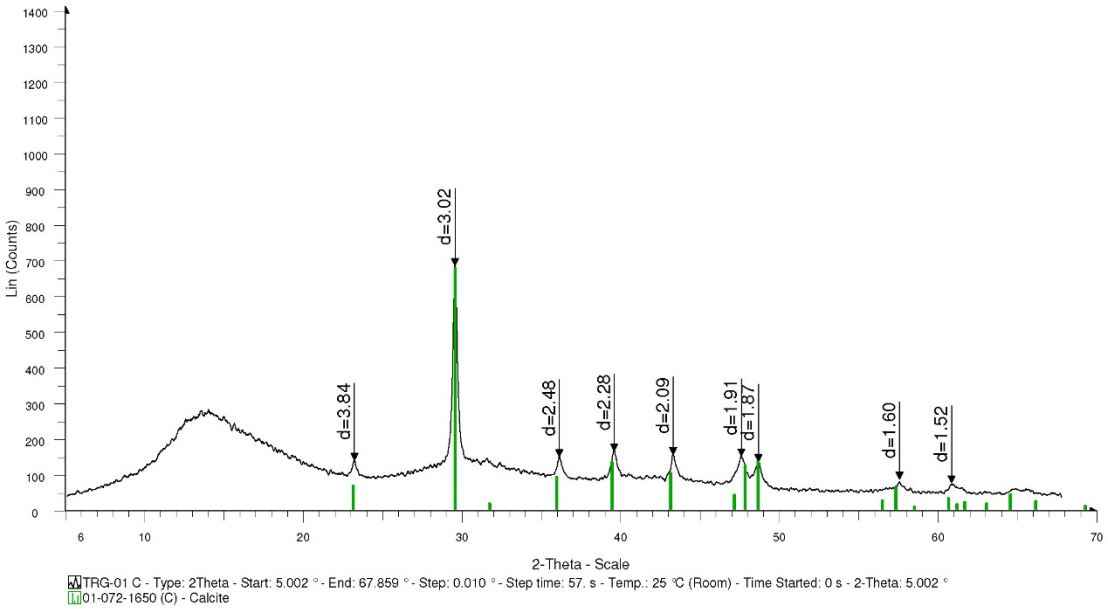

TRG-02

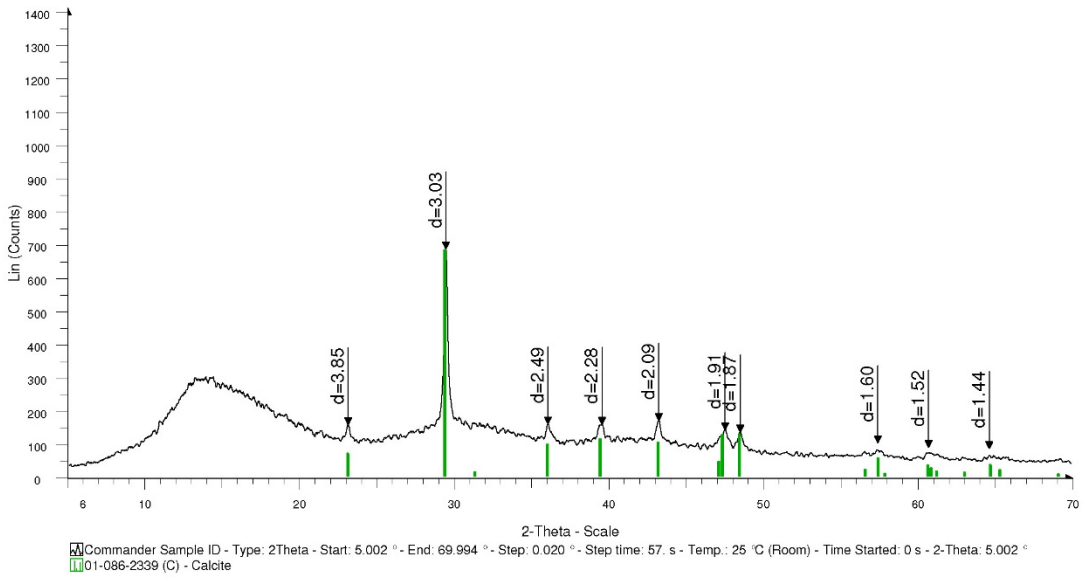

TRG-03 A

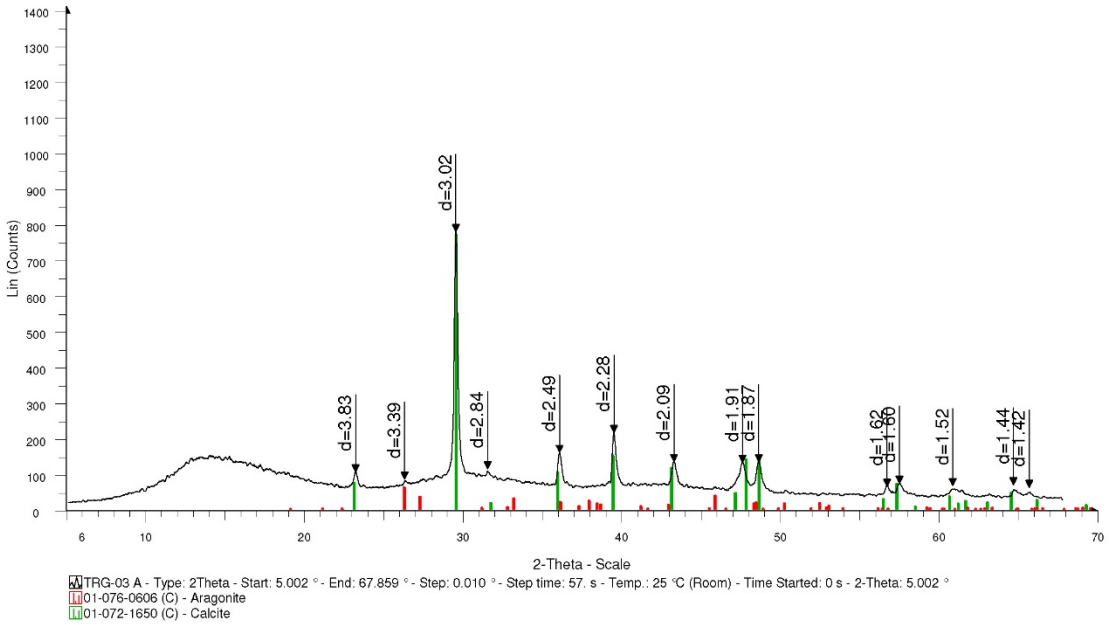

TRG-03 B

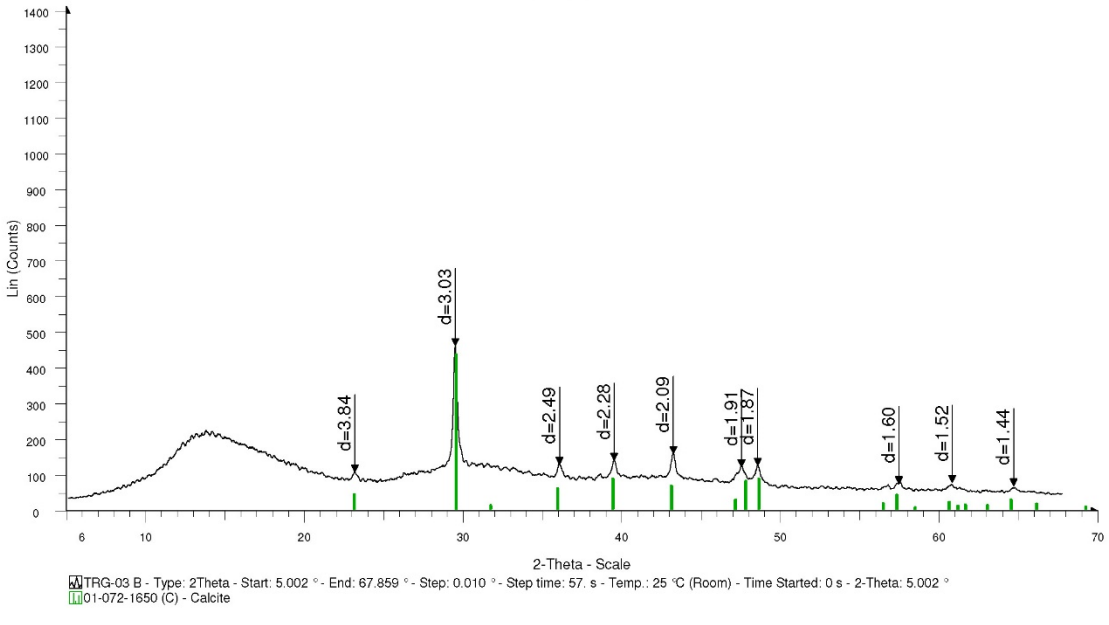

TRG-03 C

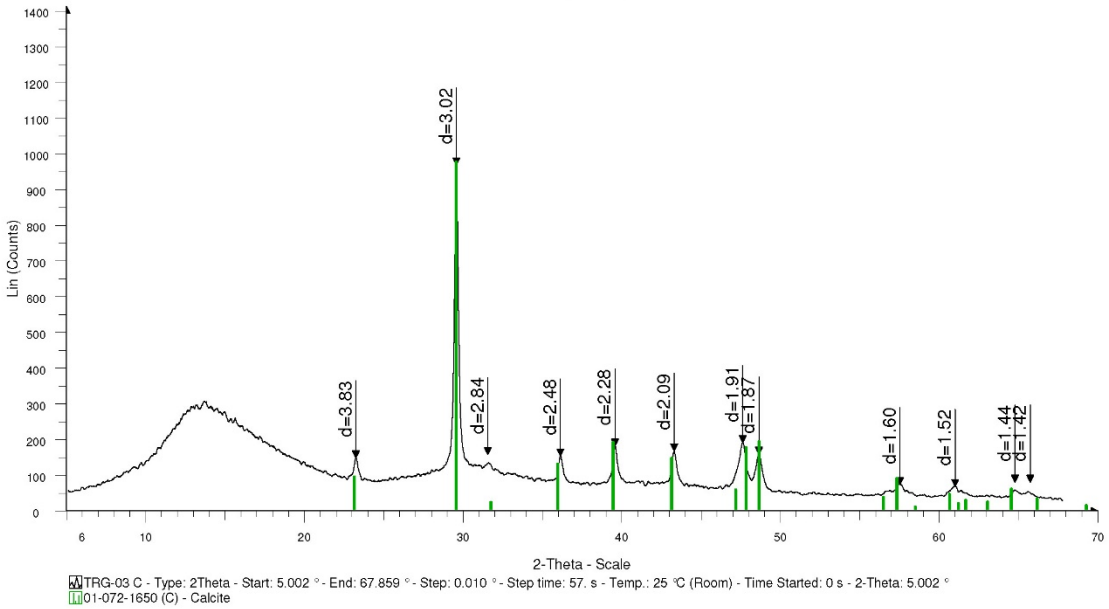

TRG-04 A

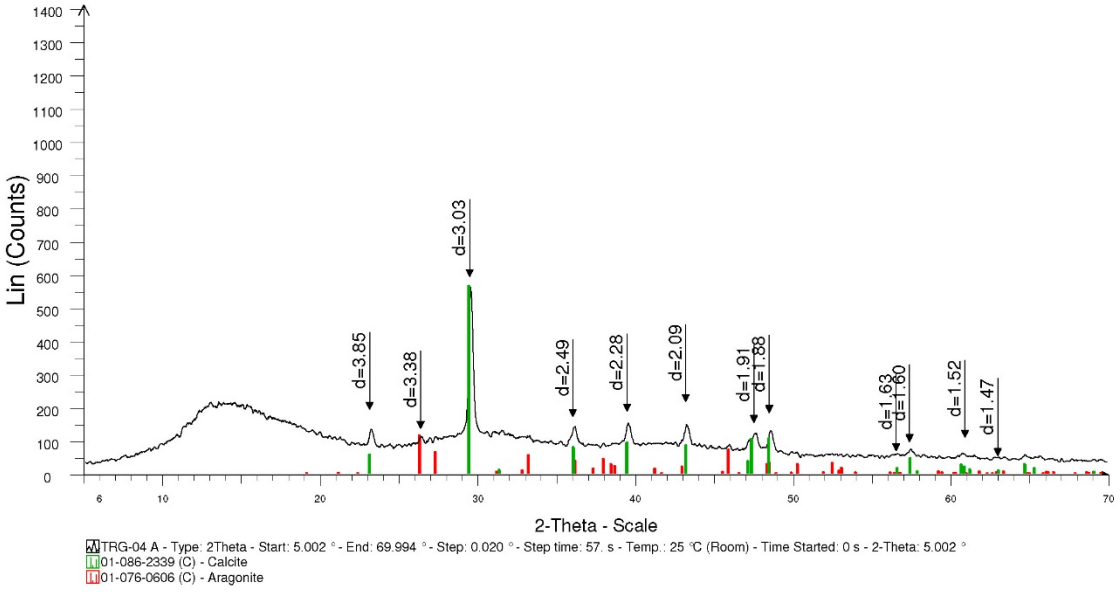

TRG-04 B

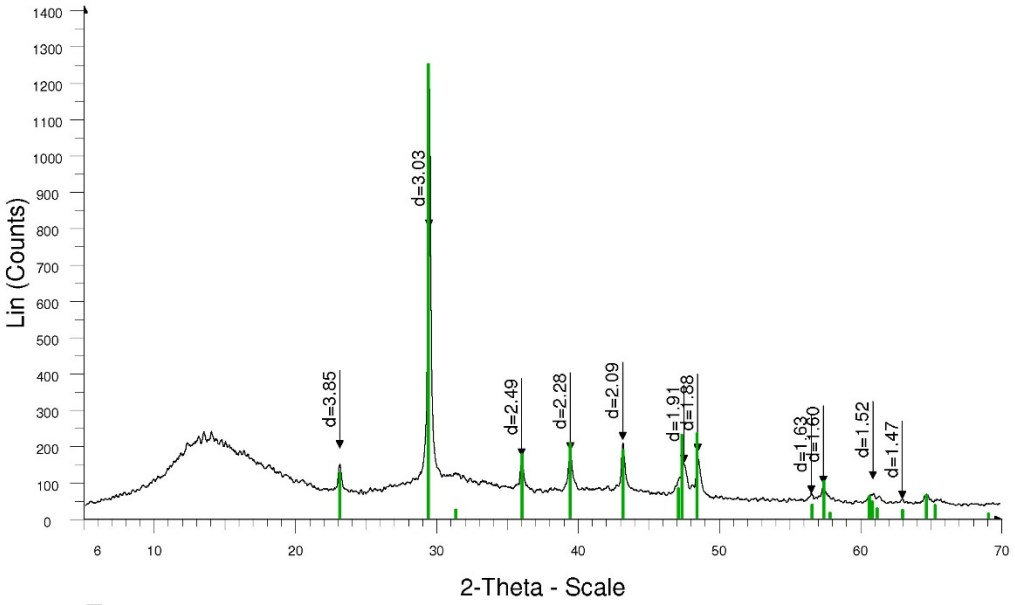

TRG-04 B - Type: 2Theta - Start: 5.002 ° - End: 69.994 ° - Step: 0.020 ° - Step time: 57. s - Temp.: 25 °C (Room) - Time Started: 0 s - 2-Theta: 5.002 °
Operations: Smooth 0.150 | Import
01-086-2339 (C) - Calcite

TRG-04 C

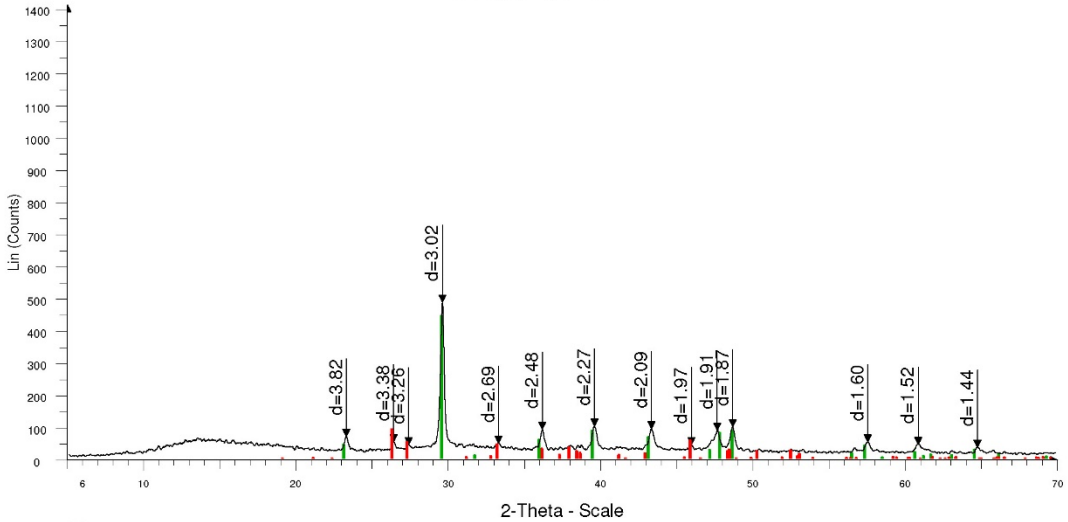

TRG-04 C - Type: 2Theta - Start: 5.002 ° - End: 69.994 ° - Step: 0.020 ° - Step time: 57. s - Temp.: 25 °C (Room) - Time Started: 0 s - 2-Theta: 5.002 °
01-076-0606 (C) - Aragonite
01-072-1650 (C) - Calcite

TRG-04 D

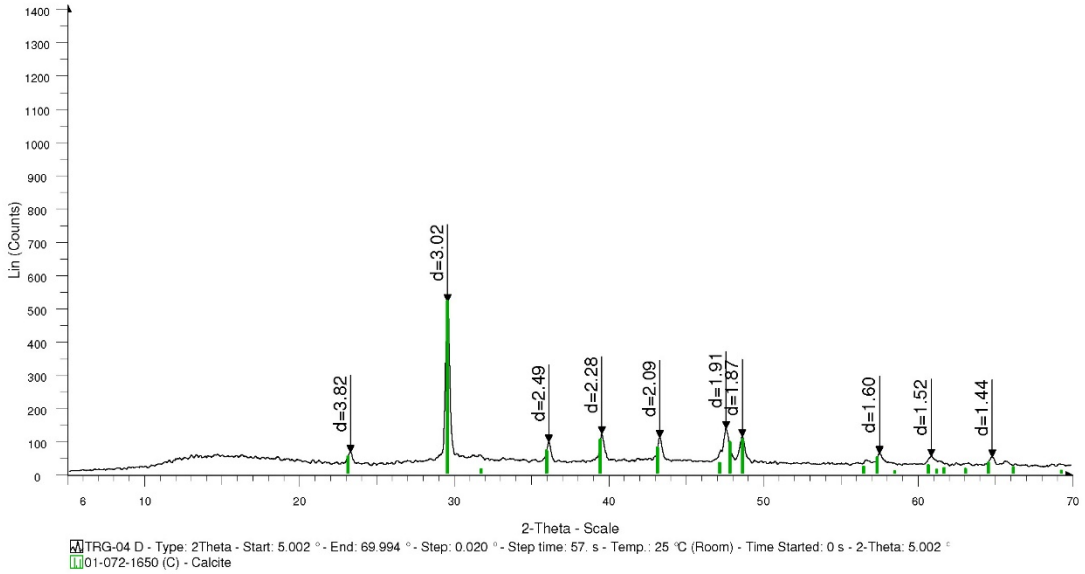

TRG-05

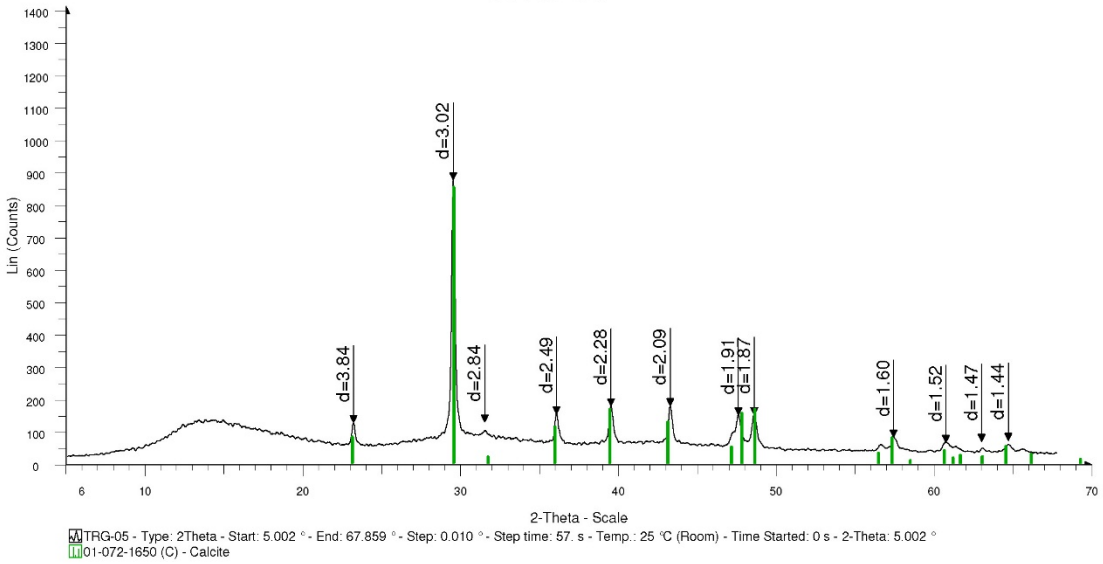

Supplementary Figure S9: a) Short columnar calcite crystals alternating with brown micritic bands constitute the first calcite precipitates over the host rock. Plane polarised light (PPL); b) columnar calcite crystals predominantly oriented towards the right (downslope). The growth of the crystal on the center crosscut the direction of growth of previous crystals. Crossed polarised light (XPL); c) oriented columnar calcite crystals displaying signs of dissolution. Occasionally, both crystal layers are separated by a thin, wavy micritic layer possibly indicating dissolution processes (PPL); d) aragonite-calcite layered textures (right) and secondary calcite crystals with aragonite relicts, some of them arranged in fans aligned forming a band (PPL); e) secondary calcite showing abundant aragonite relicts and very anhedral textures (PPL); f) same image as e, under crossed polarised light.

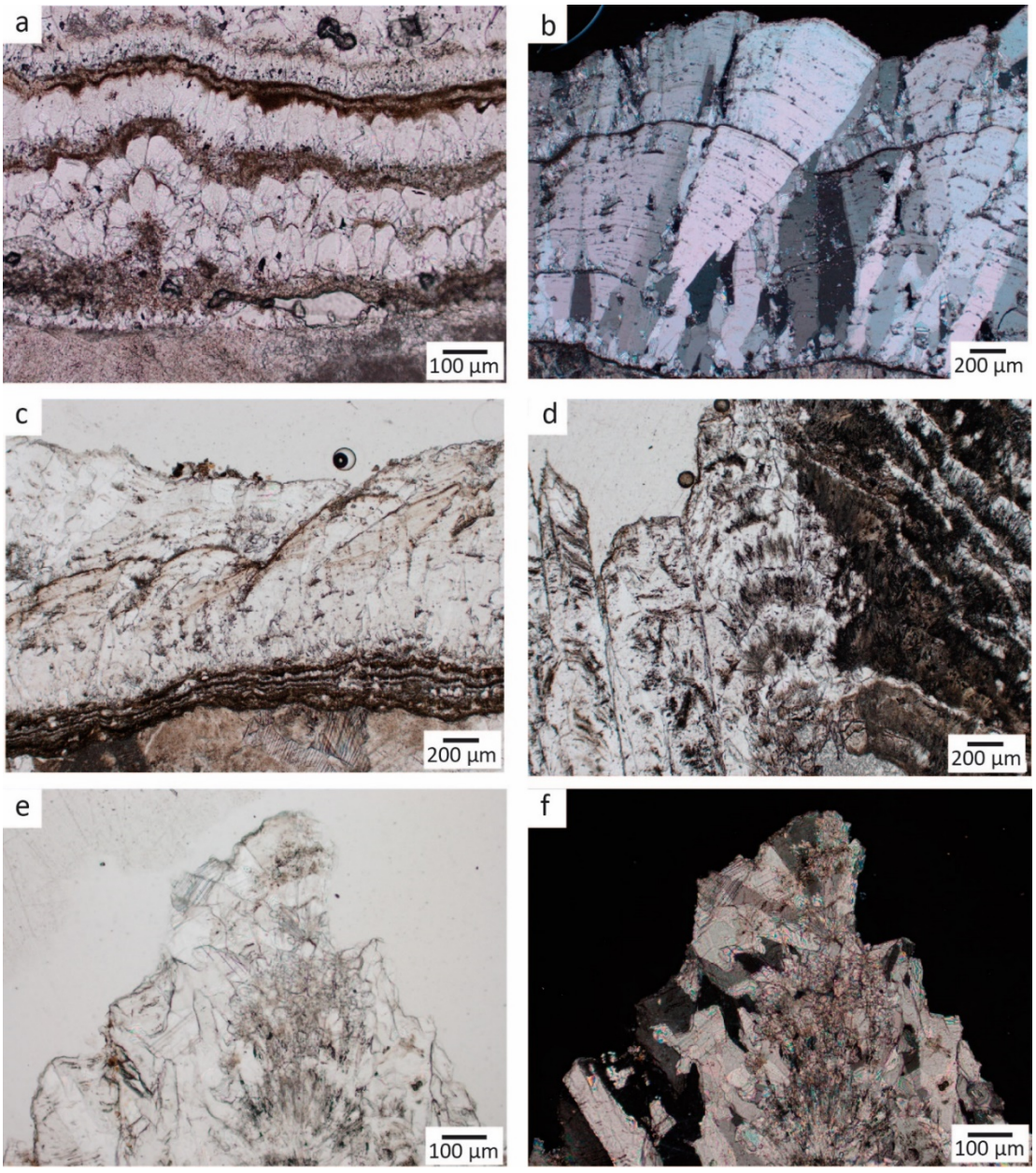

Supplementary Figure S10: The columnar and elongated columnar calcites oriented downslope (plane polarised light – above, and crossed polarised light – below)

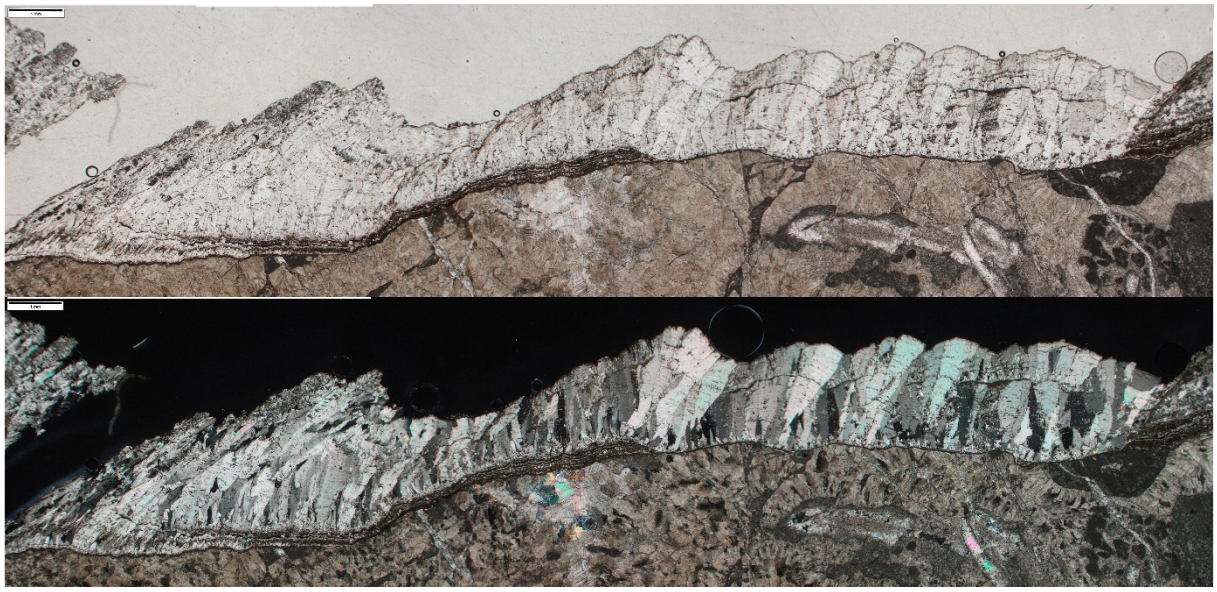

Supplementary Figure S11: The photograph and ^{14}C results of dated moraine organic matter by Karsten Grunewald and his team in the laboratory in Erlangen.

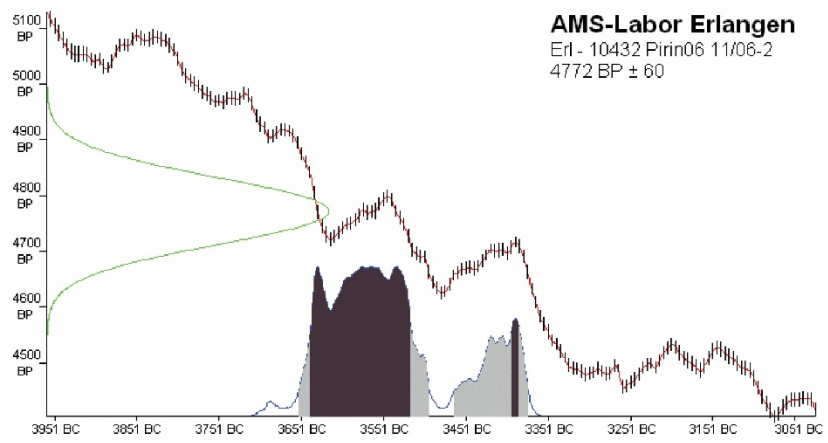

Die Probe wurde gemessen zu 4772 ± 60 Radiokarbonjahren.

Das entspricht einem kalibrierten Alter in folgenden Bereichen:

Mit 68,3 % Wahrscheinlichkeit (1 Sigma):

3640 BC - 3519 BC	65,6%
3395 BC - 3388 BC	2,7%

Mit 95,4 % Wahrscheinlichkeit (2 Sigma):

3654 BC - 3496 BC	74,3%
3465 BC - 3376 BC	21,1%

Kalibrierungsdatensatz aus: Reimer et al., IntCal04 Terrestrial Radiocarbon Age Calibration, 0–26 cal kyr BP, Radiocarbon; 46; (3); (2004), 1029 - 1058; ""

Supplementary Table S1: $\delta^{13}C$ and $\delta^{18}O$ stable isotope ratios.

Sample	$\delta^{13}C$ (‰ PDB)	$\delta^{18}O$ (‰ PDB)
T.01_a	2.41	-2.84
T.03_a	1.35	-4.71
T.03_b	0.51	-5.45
T.04_c	1.50	-3.96
T.05_a	0.98	-4.63

Supplementary Table S2: U-Th data for the subglacial calcite. Note: Ratios in parentheses are activity ratios calculated from the atomic ratios. Errors are at 2δ level. The ages are calculated using the Isoplot 3.75 Program of Ludwig (2012)(Ludwig, 2012) with decay constants from Cheng et al. (2000)(Cheng et al., 2000). Corrected Ages were calculated assuming initial/detrital $^{230}Th/^{232}Th$ activity ratio equal 0.825 ± 50 % (the bulk-Earth value, which is the most commonly used for initial/detrital ^{230}Th corrections).

U-Th dating was carried out using a Nu Plasma multi-collector inductively-coupled plasma mass spectrometer (MC-ICP-MS) in the Radiogenic Isotope Facility (RIF) at the School of Earth and Environmental Sciences, The University of Queensland (UQ) following chemical treatment procedures and MC-ICP-MS analytical protocols described elsewhere(Clark et al., 2012; Clark et al., 2014; Zhao et al., 2009). Powdered or chipped sub-samples weighing 16–78 mg were spiked with a mixed ^{229}Th-^{233}U tracer and then completely dissolved in concentrated HNO_3. After digestion, each sample was treated with H_2O_2 to decompose trace amounts of organic matters (if any) and to facilitate complete sample-tracer homogenisation. U and Th were separated using conventional anion-exchange column chemistry using Bio-Rad AG 1-X8 resin. After stripping off the matrix from the column using double-distilled 7N HNO as eluent, 3 ml of a 2% HNO_3 solution mixed with trace amount of HF was used to elute both U and Th into a 3.5-ml pre-cleaned test tube, ready for MC-ICP-MS analyses, without the need for further drying down and re-mixing. After column chemistry, the U-Th mixed solution was injected into the MC-ICP-MS through a DSN-100 desolvation nebuliser system with an uptake rate of around 0.07 ml per minute. U-Th isotopic ratio measurement was performed on the MC-ICP-MS using a detector configuration to allow simultaneous measurements of both U and Th isotopes(Clark et al., 2014; Zhou et al., 2011). The $^{230}Th/^{238}U$ and $^{234}U/^{238}U$ activity ratios of the samples were calculated using the decay constants given in(Cheng et al., 2000). The non-radiogenic ^{230}Th was corrected using an assumed bulk-Earth atomic $^{230}Th/^{232}Th$ ratio of $4.4\pm2.2\times10^{-6}$. U-Th ages were calculated using the Isoplot/Ex 3.75 Program(Ludwig, 2012).

Sample Name	Sample wt.(g)	U (ppm)	±2s	^{232}Th (ppb)	±2s	(^{230}Th/^{232}Th)	±2s	(^{230}Th/^{238}U)	±2s	(^{234}U/^{238}U)	±2s	uncorr. ^{230}Th Age (ka)	±2s	corr. ^{230}Th Age (ka)	±2s	corr. Initial (^{234}U/^{238}U)	±2s
T.01_a1	0,06022	0,45584	0,00019	20,522	0,019	10,945	0,047	0,1624	0,0007	0,9787	0,0012	19,83	0,10	**18,45**	**0,70**	0,9773	0,0013
T.03_a1	0,07823	0,41066	0,00017	7,454	0,012	19,219	0,103	0,1150	0,0006	1,0053	0,0005	13,26	0,07	**12,72**	**0,28**	1,0055	0,0006
T.03_a2	0,02380	0,8933	0,0003	4,929	0,005	19,99	0,23	0,0363	0,0004	1,0062	0,0011	4,012	0,047	**3,849**	**0,094**	1,0063	0,0011
T.03_b1	0,01620	1,7737	0,0005	4,080	0,005	24,49	0,23	0,0186	0,0002	1,0079	0,0008	2,027	0,019	**1,959**	**0,039**	1,0079	0,0008
T.05	0,02151	1,3305	0,0004	68,59	0,11	12,20	0,05	0,2072	0,0008	1,0060	0,0010	25,15	0,11	**23,62**	**0,78**	1,0065	0,0011
HU-1 standard	0,03057	0,7511	0,0003	0,0660	0,0006	34680	342	1,0036	0,0026	1,0013	0,0011	**Secular equilibrium**					
HU-1 standard	0,03538	0,7542	0,0003	0,1994	0,0008	11439	53	0,9969	0,0024	1,0006	0,0009	**Secular equilibrium**					
YB-1 standard	0,09094	0,1293	0,0001	0,5889	0,0012	291,3	1,3	0,4371	0,0018	1,7452	0,0018	30,79	0,15	**30,71**	**0,15**	1,8136	0,0020
YB-1 standard	0,10259	0,1292	0,0001	0,6118	0,0012	278,6	1,3	0,4348	0,0019	1,7445	0,0020	30,62	0,15	**30,54**	**0,16**	1,8126	0,0022
SRM-960 standard	0,10570	5,5396	0,0046	0,01	0,000	1485	28	0,00071	0,00001	0,9636	0,0007	0,0805	0,0009	**0,0805**	**0,0009**	0,9636	0,0007
YB-1 speleothem std	0,10214	0,1253	0,0000	0,49	0,001	339,8	1,2	0,4343	0,0015	1,7492	0,0013	30,53	0,12	**30,46**	**0,12**	1,8174	0,0014

REFERENCES:

Cheng, H., Edwards, R. L., Hoff, J., Gallup, C. D., Richards, D. A., and Asmerom, Y.: The half-lives of uranium-234 and thorium-230, Chemical Geology, 169, 17-33, doi:10.1016/s0009-2541(99)00157-6, 2000.

Clark, T. R., Zhao, J.-x., Feng, Y.-x., Done, T. J., Jupiter, S., Lough, J., and Pandolfi, J. M.: Spatial variability of initial $^{230}Th/^{232}Th$ in modern Porites from the inshore region of the Great Barrier Reef, Geochimica et Cosmochimica Acta, 78, 99-118, doi:10.1016/j.gca.2011.11.032, 2012.

Clark, T. R., Zhao, J.-x., Roff, G., Feng, Y.-x., Done, T. J., Nothdurft, L. D., and Pandolfi, J. M.: Discerning the timing and cause of historical mortality events in modern Porites from the Great Barrier Reef, Geochimica et Cosmochimica Acta, 138, 57-80, doi:10.1016/j.gca.2014.04.022, 2014.

Gabrovec, M., Hrvatin, M., Komac, B., Ortar, J., Pavšek, M., Topole, M., Triglav Čekada, M., and Zorn, M.: Triglavski ledenik, Založba ZRC, Ljubljana, 2014.

Ludwig, K. R.: User's manual for Isoplot version 3.75–4.15: a geochronological toolkit for Microsoft Excel, Berkeley Geochronological Center Special Publication, 5, 2012.

Zhao, J.-x., Yu, K.-f., and Feng, Y.-x.: High-precision ^{238}U–^{234}U–^{230}Th disequilibrium dating of the recent past: a review, Quaternary Geochronology, 4, 423-433, doi:10.1016/j.quageo.2009.01.012, 2009.

Zhou, H., Zhao, J., Qing, W., Feng, Y., and Tang, J.: Speleothem-derived Asian summer monsoon variations in Central China, 54-46 ka, Journal of Quaternary Science, 26, 781-790, doi:10.1002/jqs.1506, 2011.